www.czasopisma.pan.pl PAN POLSKA AKADEMIA NAUK www.journals.pan.pl

Arch. Min. Sci. **69** (2024), 2, 303-325

Electronic version (in color) of this paper is available: http://mining.archives.pl

DOI: https://doi.org/10.24425/ams.2024.150347

KUNYOU ZHOU[1*], JIAXUAN WU[1], JILIANG KAN[1], KE YANG[1], XIANGZHUO ZHAO[2], YUNPENG LI[3]

BOLTING CONTROL OF A COAL ROADWAY UNDER MULTI-SEAM MINING – A CASE STUDY

The stress field of the roadway under multi-seam mining is complex due to multiple mining disturbances. The bolting control of the roadway under multi-seam mining has attracted wide concern. Moreover, conventional metal supporting materials in the coal rib are prone to sparks when shearer works, and new bolting materials are urgently needed. Taking a track roadway under multi-seam mining in China as the engineering case, the mining-induced stress field of the track roadway under multi-seam mining was investigated through numerical simulation and lab and field tests. The test evaluated the mechanical behaviour of FRP bolts and rebar bolts, as well as their anchorage performance under different conditions. Comparative analysis was conducted on the deformation and failure characteristics of the roadway under different bolting parameters to determine an optimised bolting scheme for the track roadway in the I011501 working face. The results show that the goafs and the remaining coal pillars in the overlying coal seams increase the stress in the track roadway in the I011501 working face, especially for the lower rib and roof. The tensile force of the 27 mm-diameter FRP bolt is 1.2 times that of the 22 mm-diameter rebar bolt. The shear strength of the full-length anchored FRP bolt is 70.8% higher than that of the end-anchored bolt. The peak stress of the full-length-anchored bolt is in the shallow coal and rock mass. The optimised bolting scheme of the track roadway subject to multi-seam mining is determined, and the cost of the optimised bolting scheme is lower by about 25.2%, as compared with the primary bolting scheme. Numerical simulation and field application results indicate that the optimised bolting scheme can significantly reduce the deformation and plastic failure of the track roadway in the I011501 working face, which is under multi-seam mining conditions.

Keywords: multi-seam mining; coal roadway; bolting support; mining-induced stress; FRP bolt; full-length anchorage

[1] ANHUI UNIVERSITY OF SCIENCE AND TECHNOLOGY, KEY LABORATORY OF SAFETY AND HIGH-EFFICIENCY COAL MINING, MINISTRY OF EDUCATION, CHINA
[2] SHAANXI YANCHANG PETROLEUM BALASU COAL INDUSTRY LIMITED COMPANY, CHINA
[3] CHINA COAL RESEARCH INSTITUTE, CHINA

* Corresponding author: TB18020033B4@cumt.edu.cn

1. Introduction

There are multiple mineable coal seams within close distance in the Datong, Xinwen, Pingdingshan, and Huainan areas in China and other coal-producing countries [1-3]. The overburden strata structure in mines where multiple coal seams are mined is complex due to the influence of mining disturbances. The goafs and residual coal pillars in the upper coal seams cause the stress field in the lower working face and roadway to become complex, which results in the formation of strong mine pressure and the instability of roadways [4,5], whose manifestations include the frequent occurrence of severe roof subsidence and rib swelling, among others. Therefore, the stability and bolting support of roadways in lower coal seams under multi-seam mining is increasingly attracting more attention.

Many studies have focused on the structure of the overburden strata and the mining-induced stress field under multi-seam mining conditions [6]. Ghabraie et al. [7,8] found that the panel layouts in two adjacent coal seams seriously affected the multi-seam subsidence and put forward a robust FEM-based modelling method to simulate the strata movement above the multi-seams. Huang et al. [9] investigated the failure characteristics of intermediate strata having different offset distances between coal pillars in the upper and lower seams. Tian et al. [10] studied the stability of roof strata and coal pillars during multi-seam mining and found that the multi-seam mining aggravated the roof damage and that the remaining coal pillars resulted in stress concentration in the lower working face. Liu et al. [11] investigated the mining process of the lower coal seam in multiple seams. The findings of the investigation showed that during the mining of the lower coal seam, the fracture zone in the upper goaf was converted into a caving zone, and the permeability and the number of fractures in the overlying strata were of a pattern of "stability-rapid increase-stability". Adhikary et al. [12] found that 3D numerical models were better suitable for the overlying strata movement and the stress field in surrounding rock. Suchowerska et al. [13] carried out finite element modelling and found that multi-seam mining could not lead to a significant increase in horizontal stress. Zhang et al. [14] found that the vertical stress in the strata under a protective mined seam reduced significantly; however, the lateral stress increased with depth and became concentrated in the lower section. Wang et al. [15] found that the stress and deformation of a roadway under a coal pillar were stronger than that under the gobs and solid coal; based on these results, optimal bolting support parameters were simulated and determined.

The mechanical behaviour of different bolts and bolting structures in roadways under complex stress fields has been tested, and a variety of supporting technologies and bolting materials have been proposed and applied in the field [16]. Pedersen et al. [17] tested the stress distribution in bolts and nuts and found that the maximum stress in the bolt is at the fillet under the head, at the thread start, or at the thread root. Sarfarazi et al. [18] tested the effect of loading rate on the interaction between rock bolts and rock bridges. Yang et al. [19] found that the efficiency of the torque conversion into the bolt preload of steel bolts was higher than that in the fibre-reinforced polymer (FRP) bolts and that the steel bolt could significantly increase jointed rock mass capacity. Majcherczyk et al. [20] conducted field monitoring over several years and confirmed the effectiveness of combined yielding steel arch with rock bolt support systems. Moffat et al. [21] indicated that the optical fibre could be used to monitor the strain and the stress in the bolts under loading conditions and estimate the behaviour of rock mass during mining. Zhang et al. [22] proposed a new prestressed yield bolt after considering the breakage characteristics of the bolt and the instability of deep and highly stressed roadways. Małkowski et al. [23] conducted laboratory tests and numerical modelling on the mechanical behaviours of bolts with three bond types of

resin, organic mineral glue and cement bond. Sun et al. [24] developed a new numerical model for analysing the tension-shear coupling fracture behaviour of rock bolts and proposed a new mechanical criterion and constitutive model of the yield and fracture of rock bolts. Lawler et al. [25] developed a novel FRP bolt with mechanical anchorages and put forward a new anchorage technique for the FRP rods. Abdelkerim et al. [26] studied the effect of bolt types on the static and fatigue performance of basalt fibre-reinforced polymer (BFRP) multi-bolted double-lap connections. Han et al. [27] and Feng et al. [28] tested the mechanical properties of an FRP bolt and concluded that large-diameter FRP bolts could be used for effective rib support in large-deformation roadways. Tin et al. [29] used the topology optimisation technique to optimise the bolting reinforcement scheme for underground excavation, including the bolting pattern, spacing, and size. Ghyasvand et al. [30] adopted the TOPSIS Fuzzy method for the optimisation of the reinforced supporting systems of an old tunnel in Iran.

The determination of the bolting scheme in previous cases mostly relied on engineering experience, which usually ignored the mining influence from adjacent coal seams and other new support materials. In this study, the stress field induced by multi-seam mining conditions in a typical roadway was investigated. Subsequently, the anchorage performance of FRP and rebar bolts was tested under different anchorage conditions. After this, the optimal bolting parameters of the roadway were comparatively analysed, and finally, an optimised bolting scheme was determined and applied in the field.

2. Study Area

2.1. Layout of the mine with the multi-seam mining conditions

The studied coal mine is being mined by the National Energy Group Xinjiang Energy Co. LTD. It is located in the west of the Liuhuanggou mining area in the Zhunnan coalfield, China and 40 km from Urumqi. Moreover, it is a high-gas coal mine. There are four mineable coal seams, named 4#-5#, 9-10#, 14#, and 15#, with average thicknesses of 7.6 m, 8.9 m, 9.1 m and 11.2 m, respectively. The dip angle of the coal seams is 10°-25°. The fully mechanised top coal caving method is adopted for coal mining, and the goaf is managed using the full caving method.

The average thickness, dip angle, burial depth, and original gas content of the M15 coal seam in the I011501 working face are 10.1 m, 16°, 440 m, and 1.20-2.08 m^3/t, respectively. The lengths of the working face in the inclination and strike directions are 205.6 m and 876 m, respectively. The I011501 working face is located under the goafs in the 4-5#, 9-10#, and 14# coal seams. The track roadway in the I011501 working face, with a depth of 405 m, is 80 m, 53 m, and 18 m from the overburden in the 4-5#, 9-10#, and 14# coal seams, respectively. The track roadway in the horizontal direction is 45 m away from the remaining coal pillar in the 14# coal seam. The spatial-temporal relationship between the track roadway and the working faces in the overburden is shown in Fig. 1.

It can be seen that the working faces in the overburden 4-5# and 9-10# coal seams were mined before the excavation of the track gateway. The mining of the I011401 working face occurred before the excavation of the track roadway in the I011501 working face, and the mining of the I011402 working face lags behind the excavation of the track roadway. The track roadway in the I011501 working face is under complex stress conditions caused by the presence of the overburdened goafs and the remaining coal pillars.

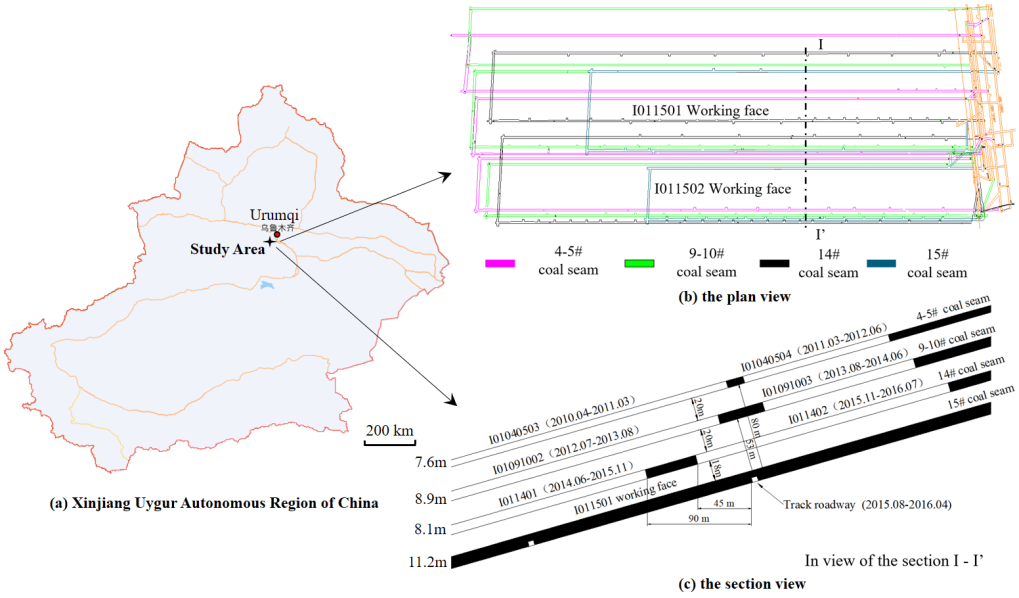

Fig. 1. Spatial-temporal relationship of the track roadway and the overburdens of the working faces

2.2. Stability of the track roadway under multi-seam mining

The track roadway in the I011501 working face was driven along the floor of the coal seam, and it is a three-centered arch 4.3 m wide and 3.5 m high. The track roadway is supported by bolts and cables, as shown in Fig. 2. A total of thirteen rebar bolts of Φ22 × 3000 mm have been

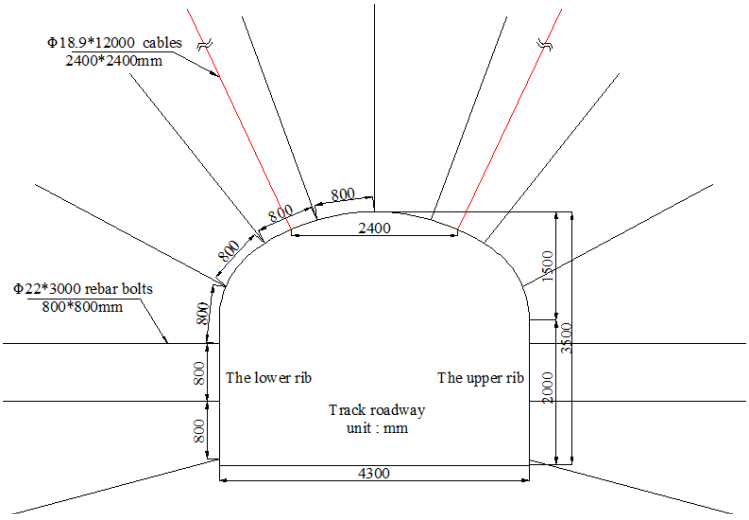

Fig. 2. Bolting scheme of the track roadway under multi-seam mining

installed in a section of the roadway. Of these, five are in the roof, and eight are in the two ribs. The spacing between the bolts is 800 mm × 800 mm. Each bolt is anchored with three CK23-35 resin cartridges. A total of two steel strand cables of Φ18.9 × 12000 mm have been installed in the roof with a spacing of 2400 mm × 2400 mm, and they are anchored with eight CK23-35 resin cartridges. Meanwhile, a cold-drawn wire mesh with a size of 3400 mm × 1000 mm has been used on the surface of the track roadway.

The overburden goafs and remaining coal pillars have caused the track roadway in the I011501 working face to seriously deform, and roof subsidence and rib swelling have occurred frequently, with the maximum rib swelling reaching 100 cm, as shown in Fig. 3. According to the SIR-20 geological radar detection results, the depths of the loose zones in the upper rib, roof strata, and lower rib of the track roadway are 2.0 m, 1.8 m, and 2.4 m, respectively. Therefore, the bolting scheme of the track roadway under multi-seam mining conditions needs to be further optimised for the stability of the track roadway and safe mining operations.

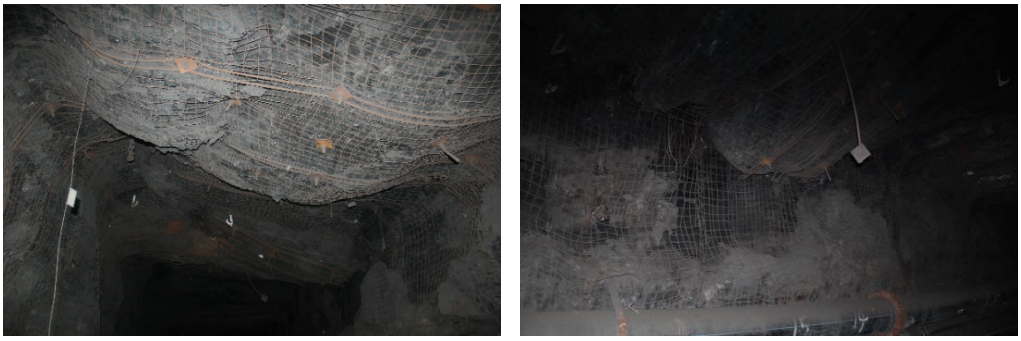

(a) roof subsidence (b) rib swelling

Fig. 3. Deformation and failure of the track roadway under multi-seam mining

3. Stress field of the track roadway under multi-seam mining

3.1. Numerical model

A numerical model was built using FLAC3D 6.0, as shown in Fig. 4, to study the stress field of the track roadway under the multi-seam mining conditions according to the spatial-temporal relationship of the track roadway and the overburden working faces shown in Fig. 1. The model is 460 m long, 400 m wide, and 355 m high, and includes 1495680 zones and 1533364 nodes. The top of the model is a free boundary, and the other boundaries of the model are constrained by displacement. The horizontal stress in the X, Y, and Z directions at the bottom of the model were set as 7.9 MPa, 9.4 MPa, and 12.0 MPa, respectively, based on the in-situ stress measured in the coal mine. Also, the three-dimensional stresses in the model all decrease in gradient in the Z direction. As a finite element method, FLAC is limited in simulating the deformation and break of overburden roof strata above goafs. In this study, the large-strain deformation mode was adopted, and allowed the large displacement and subsidence of the roof strata, which can help to obtain the real stress condition of the track roadway under the multi-seam mining [31].

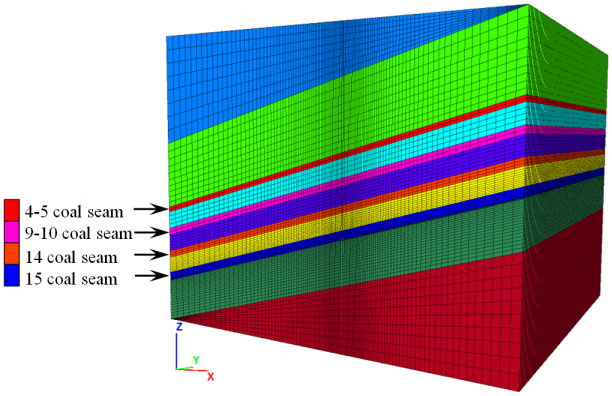

Fig. 4. Numerical model of the multi-seam mining conditions

During the numerical simulation, the mining sequence of the working faces is as follows: (1) the I01040503 and I01040504 working faces in the 4-5# coal seam; (2) the I01091002 and I01091003 working faces in the 9-10# coal seam and; (3) the I011401 and I011402 working faces in the 14# coal seam.

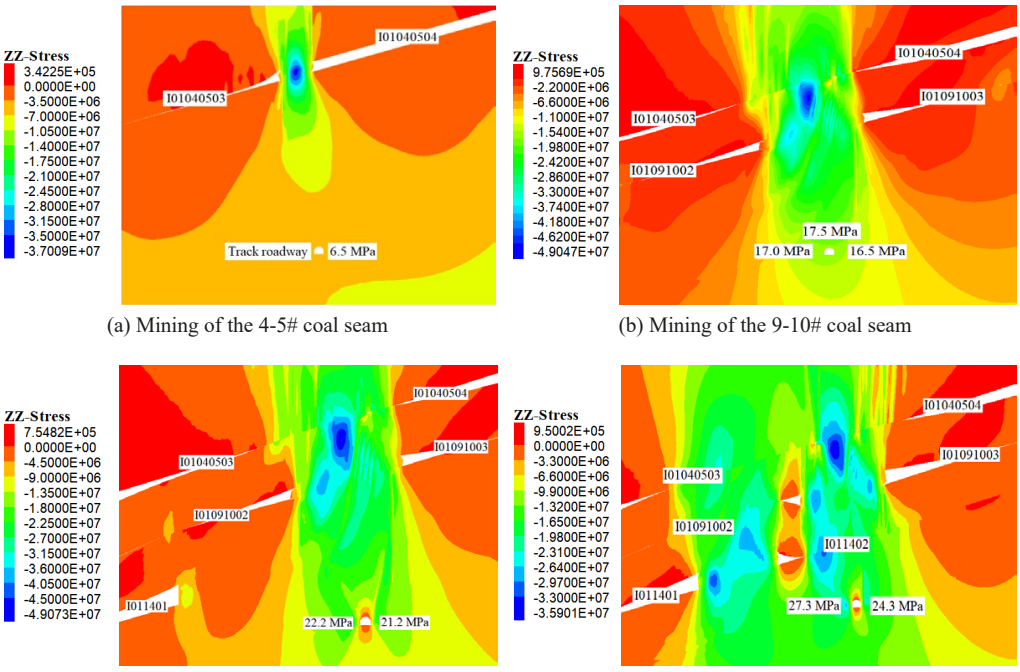

(a) Mining of the 4-5# coal seam

(b) Mining of the 9-10# coal seam

(c) Mining of the I011401 working face in the 14# coal seam

(d) Mining of the I011402 working face in the 14# coal seam

Fig. 5. Stress field of the track roadway in the I011501 working face under multi-seam mining

3.2. Numerical results

The stress field evolution in the track roadway in the I011501 working face is illustrated in Fig. 5. It can be seen that stress reduction areas in the floor are formed when the working faces in the 4-5# coal seam is mined. Meanwhile, highly concentrated stress forms in the coal pillar, the adjacent roof and the floor strata. At this moment, the track roadway of the I011501 working face is located in a stress reduction area, and its vertical stress (SZZ) and stress concentration coefficient are 6.5 MPa and 0.68, respectively. When the working faces in the 9-10# coal seam are mined, the concentrated stress in the coal pillar further increases and extends to the deeper floor strata. At this time, the track roadway is located in a high-stress area, and the SZZ and stress concentration coefficient are 17.0 MPa and 1.78, respectively. With the successive mining of the I011401 and I011402 working faces in the 14# coal seam, the SZZ stress of the track roadway increases continuously and finally reaches 27.3 MPa, with a concentration coefficient of 2.87.

Fig. 6 depicts the SZZ stress changes in the track roadway during the mining of the overburden coal seams. It can be concluded that the mining of the 4-5# coal seam 80 m above the track roadway in the I011501 working face decreases the stress level in the track roadway; this is a pressure-relieving effect. The mining of the 9-10# coal seam 53 m above the track roadway increases the stress level significantly as a result of the remaining coal pillar. Then, the stress level in the track roadway increases further with the mining of the working faces in the 14# coal seam 18 m above the track roadway. Finally, the track roadway is in a non-uniform stress field, in which the stress in the roof and lower rib is higher than that in the floor and upper rib.

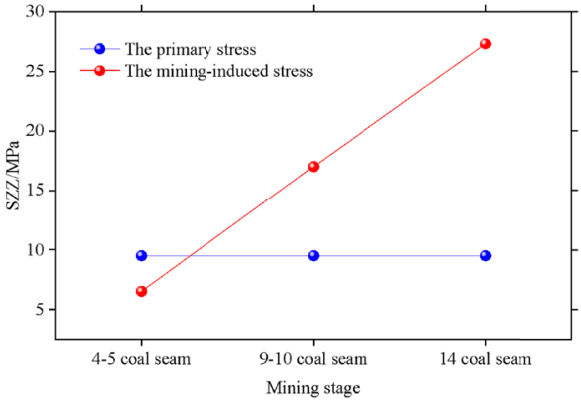

Fig. 6. The SZZ stress changes in the track roadway during the mining of the overburden coal seams

4. Experimental analysis of bolting performance

4.1. Mechanical properties of the rebar bolt and the FRP bolt

Since the 1970s, the FRP bolt has been widely used as a structural and ground reinforcing material in civil and mining fields due to its high tensile strength, good resistance to degradation and creep, low cost, and ease of being cut, as compared to conventional rebar bolts [27]. No sparks

occur during the cutting of these bolts, which is conducive to the prevention and control of gas disasters, especially in coal mines with high gas content.

The load-bearing capacity of a bolt is one of its most crucial mechanical indexes. In the laboratory, tensile tests of rebar bolts with a diameter of 22 mm and FRP bolts with a diameter of 27 mm were conducted using the WAW-600 C testing machine. It should be noted that during the tensile test of the FRP bolts, sliding of the contact surface between the bolt and the clamp occurred, and the clamping force was not enough to pull off the bolts. Later, the test was improved by processing the middle section of the FRP bolt into a D-type fan-shaped cross-section with a chord length of 24 mm. The ultimate tensile strength of the FRP bolt with a diameter of 27 mm was calculated through area conversion. The tensile test process and the ultimate failure of the rebar and FRP bolts are shown in Fig. 7.

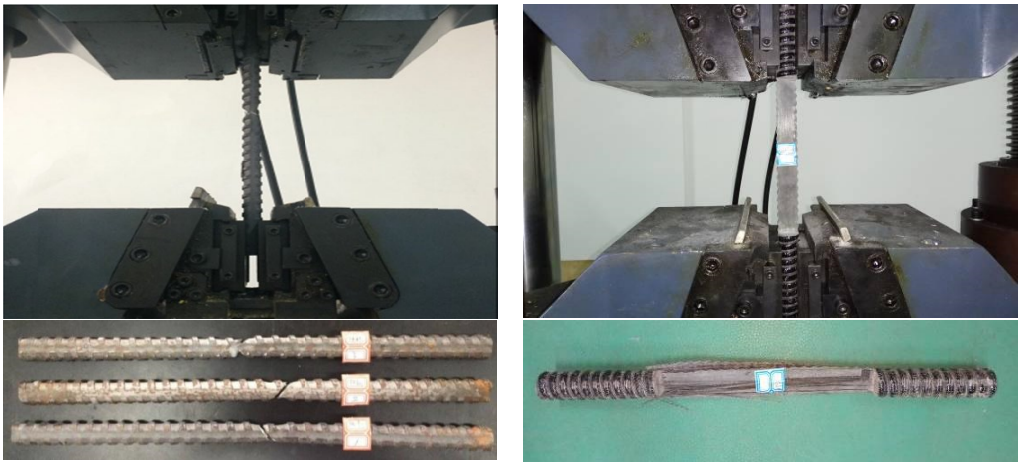

(a) rebar bolts (b) FRP bolts

Fig. 7. Tensile test process and ultimate failure of the rebar and FRP bolts

The test results are listed in TABLE 1. The ultimate tensile forces of the rebar bolt with a diameter of 22 mm and the FRP bolt with a diameter of 27 mm are 227 kN and 278.31 kN,

TABLE 1

Tensile test results of the rebar and FRP bolts

No.	Original length /mm	Extension /mm	Diameter /mm	Elongation /%		Tensile force /kN	
				Measured value	Mean value	Measured value	Mean value
R-1#	205.50	39.28	22.05	19.11	20.61	226	227
R-2#	203.20	42.40	22.10	20.86		222	
R-3#	201.56	44.10	22.08	21.87		233	
F-1#	198.10	10.14	27.01	5.10	5.70	275.23	278.31
F-2#	199.90	12.11	26.99	6.01		280.35	
F-3#	199.92	11.80	27.00	5.92		279.34	

respectively. The tensile force of the FRP bolt is 1.2 times that of the rebar bolt. However, the average elongation of the FRP bolt is 5.7%, which is much smaller than that of the rebar bolt. The tensile test indicates that the FRP bolt can be used for the effective bolting of the lower rib on the working face side.

The shear strength of a bolt is a crucial factor affecting its anchoring performance. The shear strength of bolts under different anchorage conditions was tested using a self-made double-shear testing apparatus. The anchorage condition in this study includes no anchorage, unilateral anchorage, and bilateral anchorage. All the FRP bolts were anchored for 10 minutes. During the test, the shear load was applied at a loading speed of 2 mm/min. The apparatus, test process, and failure of the bolts under different anchorage conditions are shown in Fig. 8.

The ultimate shear strength of FRP bolts under different anchorage conditions is presented in TABLE 2. It can be seen that the shear strength increases with increasing anchorage degree. Compared to the FRP bolts without any anchorage, the mean shear strengths of the bolts with unilateral anchorage and bilateral anchorage increased by 12.5% and 92.2%, respectively. There-

(a) Self-made double shear testing apparatus

(b) Shearing process

(c) Post-testing FRP bolt without anchorage

(d) Post-testing FRP bolt with unilateral anchorage

(e) Post-testing FRP bolt with bilateral anchorage

Fig. 8. Shearing test of FRP bolts under different anchorage conditions

fore, full-length anchorage can significantly increase the shear performance of FRP bolts when used for the rib support of a roadway.

The results of the pull-out test and the shearing test indicate the feasibility of using FRP bolts for roadway bolting support and provide essential parameters for the subsequent numerical simulation of bolting schemes.

TABLE 2

Shear strength of FRP bolts under different anchorage conditions

Anchorage condition	No.	Diameter /mm	Section area /mm^2	Ultimate load /kN	Ultimate strength /MPa	Mean strength /MPa
No anchorage	1#	27.1	576.80	143.22	124.15	128.24
	2#	27.1	576.80	153.56	133.11	
	3#	27.1	576.8	147.05	127.47	
Unilateral anchorage	4#	26.8	564.11	160.31	142.09	144.21
	5#	26.8	564.11	170.97	151.54	
	6#	26.8	564.11	156.82	139.00	
Bilateral anchorage	7#	26.9	568.32	251.14	220.95	246.43

4.2. Bolting performance under different anchorage lengths

To better understand the bolting performance of FRP bolts under different anchorage lengths, a 1 m × 1 m × 1 m concrete block was made in the laboratory and used to test the anchoring performance of FRP and rebar bolts with anchoring lengths of 150 mm and 300 mm. During the test, a ZY-type portable puller and a dial indicator were used to test the pull-out force and displacement, respectively. The test process is shown in Fig. 9. The pull-out force curves are shown in Fig. 10.

The ultimate pull-out force of the tested bolts is listed in TABLE 3. It can be seen that the anchoring force increases with increasing anchorage length. Compared to the 150 mm anchored

(a) Apparatus in the pull-out test (b) FRP and rebar bolts

Fig. 9. Pull-out test of the FRP and rebar bolts with different anchorage lengths

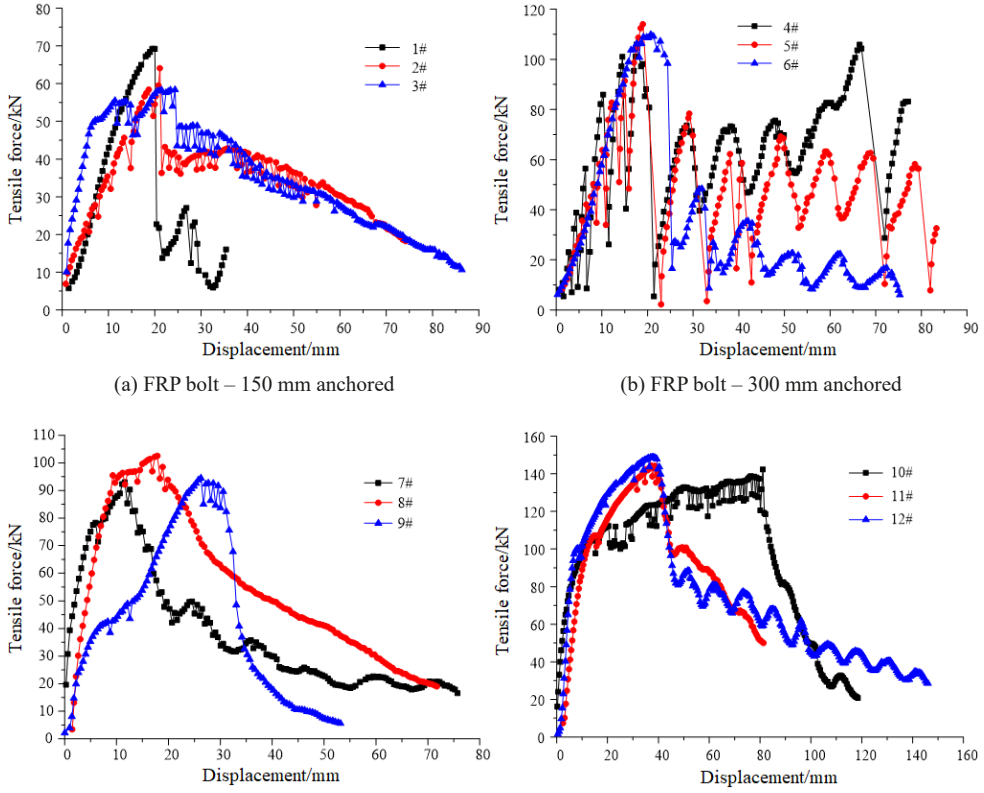

(a) FRP bolt – 150 mm anchored

(b) FRP bolt – 300 mm anchored

(c) Rebar bolt – 150 mm anchored

(d) Rebar bolt – 300 mm anchored

Fig. 10. Pull-out force curves of the FRP and rebar bolts with different anchorage lengths

TABLE 3

Pull-out force of the FRP and rebar bolts with different anchorage lengths

Type	No.	Design anchor length /mm	Real anchor length /mm	Diameter /mm	Pull-out force /kN	Mean pull-out force /kN
FRP bolt	1	150	166	27	69.2	63.9
	2		150		64.1	
	3		156		58.4	
	4	300	294		105.9	109.7
	5		289		114.0	
	6		290		109.2	
Rebar bolt	7	150	161	22	93.0	96.7
	8		178		102.5	
	9		164		94.5	
	10	300	285		142.3	145.1
	11		278		144.2	
	12		293		148.9	

bolts, the pull-out forces of the 300 mm anchored FRP bolt and rebar bolt increase by 71% and 50%, respectively. Therefore, in large-deformation roadways, increasing the anchorage length can improve the anchoring effect of the bolt. At the same anchorage length, the anchoring force of the FRP bolt is less than that of the rebar bolt. When the bolts were anchored at lengths of 150 mm and 300 mm, the mean pull-out forces of the FRP bolts were 66% and 76% of the rebar bolts, respectively. Increasing the anchorage length narrows the difference between the pull-out force of the two types of bolts. The anchorage force of the 300 mm-anchored FRP bolt reached more than 100 kN, and it can meet the requirements of roadway support. Therefore, FRP bolts with a diameter of 27 mm can be used for bolting the lower rib of track roadways under multi-seam mining.

4.3. Stress distribution in the bolts under different anchorage methods

To determine the stress distribution in end-anchored and full-length-anchored rebar bolts, field monitoring was conducted on these bolts using the Fiber Bragg Grating Sensing Technology (Fig. 11). The dimensions of the rebar bolt were φ20 mm × 2500 mm. Optical fibre was embedded in the rebar bolt. Twelve and twenty measuring points were set in the end-anchored and full-length-anchored bolts, respectively.

(a) Installation of end anchored and full-length anchored bolts

(b) Rebar bolt with optical fiber

(c) Data collection with demodulator

Fig. 11. Stress monitoring in the optical fiber rebar bolts

The stress distribution curves of the end-anchored and full-length-anchored rebar bolts in the same cross-section of a coal roadway are depicted in Fig. 12 and Fig. 13, respectively.

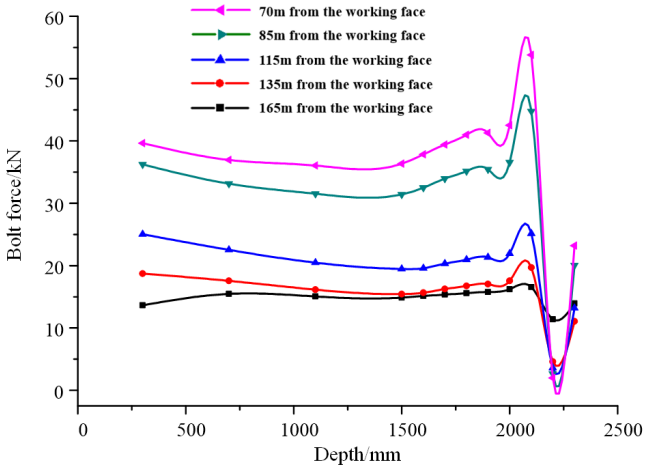

Fig. 12. Stress distribution in the end anchored rebar bolt

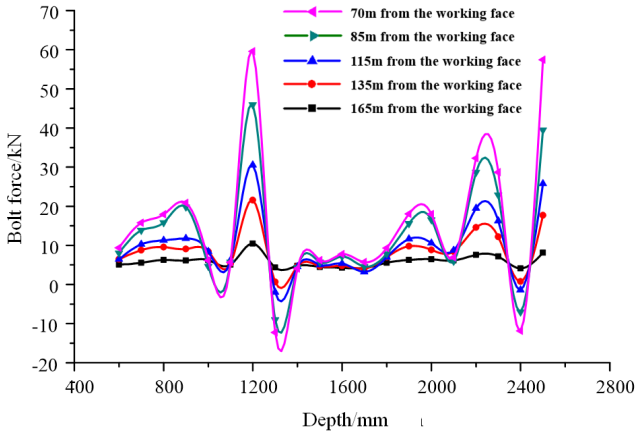

Fig. 13. Stress distribution in the full-length anchored rebar bolt

It can be seen that the stress in the non-anchored parts is uniform and that the anchored parts differ greatly; in particular, there are many stress peaks and troughs in the full-length anchored rebar bolts. This phenomenon indicates that the non-anchored parts of the end-anchored bolt are only subject to tensile force, while the anchored parts of the end-anchored and full-length-anchored bolts are not only subjected to tensile force but also to shear force caused by mutual sliding between the broken coal and rock mass. The peak stresses in the shallow rock surrounding the full-length-anchored bolt indicate that the full-length-anchored bolt can promptly inhibit the displacement of the shallow broken coal and rock mass around the roadway. Moreover, when the shallow anchorage system fails, the peak stress in the bolt is shifted to the deeper anchored parts, providing continuous anchorage. Therefore, full-length anchorage bolts can improve the stability of roadways significantly, especially in large-deformation roadways.

5. Bolting scheme optimisation

5.1. Numerical model

To optimise the bolting support parameters of the track roadway under multi-seam mining, a 34.3 m long, 50 m wide, and 33.5 m high numerical model was built, as shown in Fig. 14. The model included 760300 zones and 788205 nodes. The three-dimensional stress state of the model was derived from the large-scale numerical results in Fig. 5(d) in Section 2.2. The initial SZZ stress field was, as shown in Fig. 15, and this can more accurately reflect the stress distribution of the track roadway after the disturbance caused by the mining of the multiple overburden seams.

The Cable structural unit was used to simulate the bolts and cables in the numerical model; the two key parameters are the stiffness of the anchoring agent per unit length (k_g) and the bond strength of the anchoring agent per unit length (c_g), which can be calculated by Eq. (1) and Eq. (2) [31], respectively.

$$k_g = \frac{2\pi G}{10\ln(1+2t/D)} \tag{1}$$

where, k_g is the stiffness of the anchoring agent per unit length, N/m/m; G is the shear modulus of the anchoring agent, GPa; D is the diameter of the bolt, m; t is the thickness of the anchoring agent, m.

$$c_g = \pi(D+2t)\tau_{peak} \tag{2}$$

where, c_g is the bond strength of the anchoring agent per unit length, N/m; τ_{peak} is the peak tensile force.

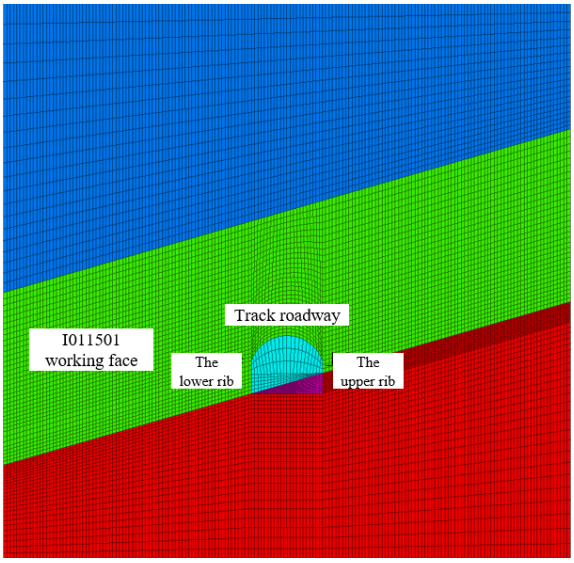

Fig. 14. Numerical model for the optimization of the bolting scheme

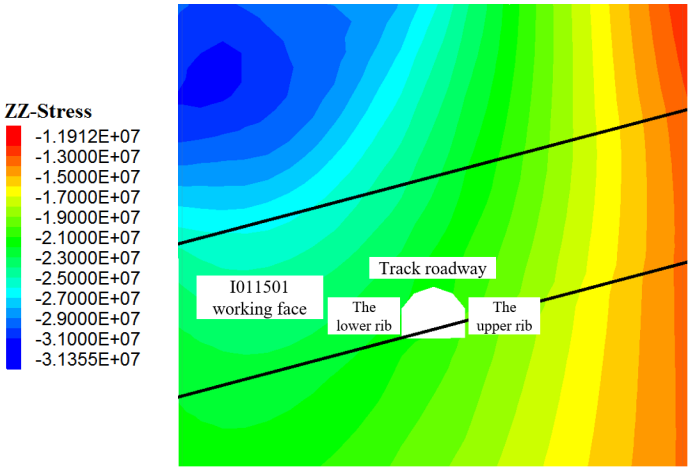

Fig. 15. Vertical stress field of the track roadway under multi-seam mining

The peak tensile force of the 22 mm diameter rebar bolt in the test mine is about 227 kN, and the tensile force of the bolt with the 0.15 m anchorage length is 97 kN. The elastic modulus and Poisson ratio of the anchoring agent are 13 GPa and 0.26, respectively. Substituting the above data into Eq. (1) and Eq. (2), k_g and c_g were calculated as 1.7×10^{10} N/m/m and 8.15×10^5 N/m, respectively. To improve the production efficiency, 27 mm diameter FRP bolts were used for the bolting of the lower rib. The peak tensile force of the FRP bolt is 280 kN and its tensile force when anchored 0.15 m is 65 kN. The parameters of the anchoring agent are the same as those of the rebar bolts. The k_g and the c_g of the FRP bolt were 1.20×10^{10} N/m/m and 4.32×10^5 N/m, respectively. The detailed Cable structural parameters are listed in TABLE 4.

TABLE 4

Cable structural parameters in the numerical model

Material	Density /(kg·m^{-3})	Elastic modulus /GPa	k_g /(N/m/m)	c_g /(N/m)	Perimeter /m	Sectional area /m^2	Maximum tensile force /kN
Rebar bolt	7900	201	1.7×10^{10}	8.15×10^5	0.069	3.80×10^{-4}	227
FRP bolt	2100	70	1.2×10^{10}	4.32×10^5	0.085	5.72×10^{-4}	280

5.2. Bolting parameters optimization

(1) Anchorage mode

The stability of the track roadway subjected to the end anchoring method and the full-length anchoring method was simulated and analyzed based on the primary bolting scheme in Fig. 2. The length of the rebar bolt was 3000 mm, and the anchoring length of the bolts was 1150 mm and 3000 mm, respectively. The plastic zone development and displacement in the surrounding rock under different anchorage conditions are shown in Fig. 16 and Fig. 17, respectively. In the figures, the black lines are bare bolts, and the white lines are anchored bolts.

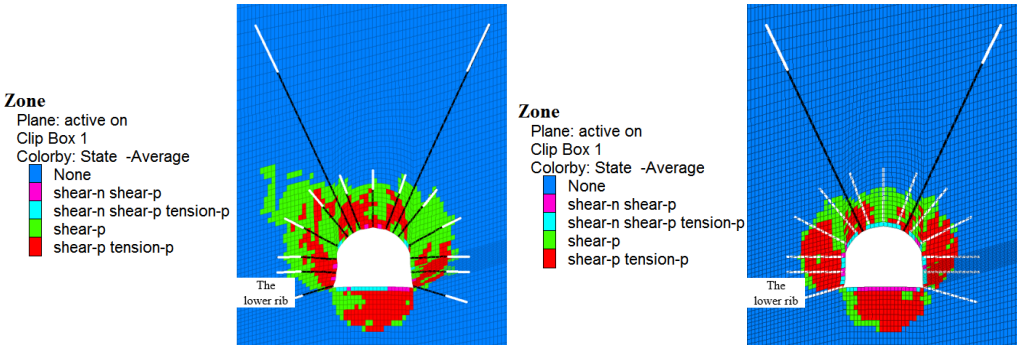

(a) End anchorage (b) Full-length anchorage

Fig. 16. Plastic zone of the roadway under different anchorage modes

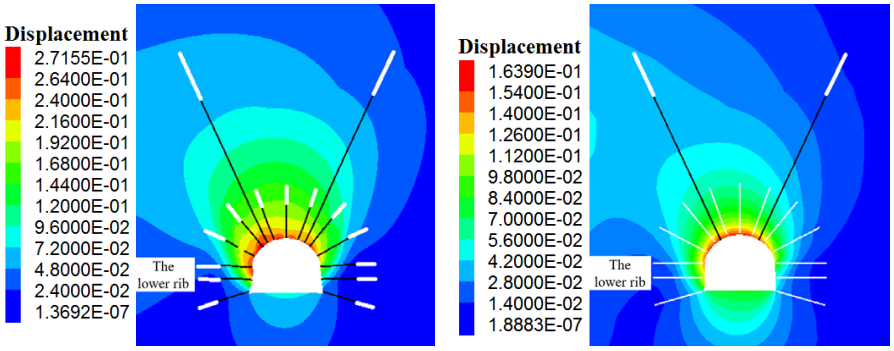

(a) End anchorage (b) Full-length anchorage

Fig. 17. Displacement of the roadway under different anchoring modes

It can be seen that both the plastic zones and the displacement of the roadway contour have a skewed distribution; the depth of the plastic zone and the displacement in the lower rib are greater than those in the upper rib as a result of the multi-seam mining in the overburden, especially when the roadway is end-anchored. A quantitative comparison of the plastic zone and the displacement of the roadway under different anchoring modes is shown in TABLE 5. Compared to the end-anchored roadway, the plastic zone depth and the displacement in the ribs and roof of the full-length-anchored roadway are both significantly reduced, while those in the roof increase slightly. It can be concluded that when the bolt is full-length-anchored, the anchorage range is

TABLE 5

Plastic zone and displacement of surrounding rock of roadway under different anchorage modes

Anchorage type	Plastic zone/m				Displacement/mm			
	Lower rib	Upper rib	Roof	Floor	Lower rib	Upper rib	Roof	Floor
End anchorage	2.6	2.4	2.2	2.0	241	132	268	72
Full-length anchorage	2.4	2.0	2.0	2.2	142	97	162	80

large, and the shear resistance is strong; this can provide effective and timely support resistance and effectively reduce the deformation and plastic zone development in the surrounding rock. Therefore, full-length-anchored bolts can be used for the bolting support of the track roadway under multi-seam mining.

(2) Bolt material

To better understand the anchoring effect of the full-length FRP bolts, 27 mm-diameter FRP bolts were used for the bolting of the lower rib, and 22 mm-diameter rebar bolts were used for the bolting of the roof and the upper rib as per the primary bolting scheme in Fig. 2. All the FRP and rebar bolts were full-length-anchored. The plastic zone development and displacement of the track roadway with different bolt materials in the lower rib are shown in Fig. 18 and Fig. 19, respectively.

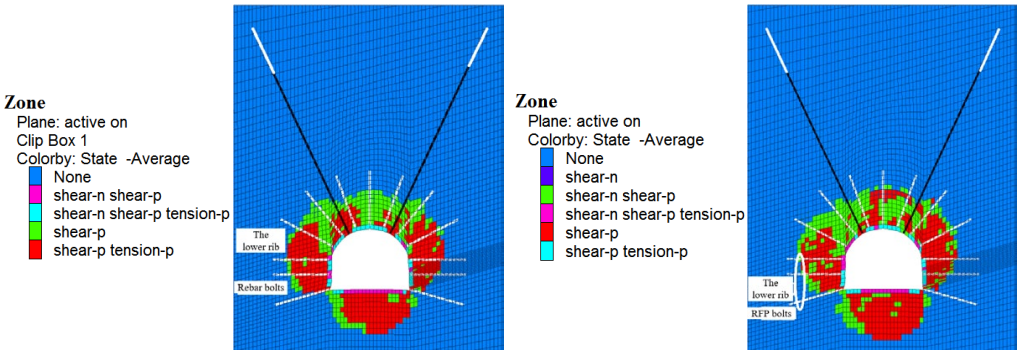

(a) Rebar bolts in the lower rib (b) FRP bolts in the lower rib

Fig. 18. Plastic zone of the roadway with different bolt material

When the FRP bolts were used in the lower rib, the depth of the plastic zone in the floor and the footing beside the lower rib, as well as the displacement, increased slightly. This phenomenon can be caused by the lower mechanical parameters of the FRP bolt than those of the rebar bolt

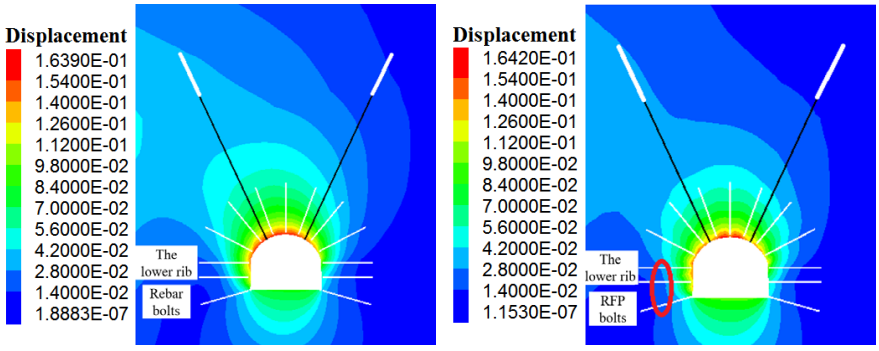

(a) Rebar bolts in the lower rib (b) FRP bolts in the lower rib

Fig. 19. Displacement of the roadway with different bolt material

in TABLE 4. However, the increase was lower than 5%, and it had little effect on the stability of the roadway. Therefore, the lower rib of the track roadway under multi-seam mining can be supported better using FRP bolts rather than rebar bolts.

(3) Parameters of the layout of the bolts and cables

Using the same numerical and analysis method above, the reasonable bolt length, spacing between bolts, row spacing, and cable number were simulated and determined, respectively. The length of the full-length anchoring FRP bolts in the lower rib was 2700 mm, and that of the full-length anchoring rebar bolts in the roof and upper rib was 2400 mm. The pitch spacing and the row spacing were both 900 mm. Three cables in a section were used in the roof, and the row spacing was 2700 mm.

5.3. The optimal bolting scheme

The optimal bolting scheme of the track roadway under multi-seam mining was determined, as shown in Fig. 20, according to the experimental and numerical results above. Five full-length-anchored rebar bolts and three rebar bolts with dimensions of Φ22×2400 mm were used in the roof and upper rib of the track roadway, respectively. Three full-length anchored FRP bolts with dimensions of Φ27×2700 mm were used in the lower rib. The pitch spacing and row spacing of the rebar bolts and the FRP bolts were both 900 mm. Three cables of Φ18.9×12000 mm were used in the roof, and their pitch spacing and row spacing were 1400 mm and 2700 mm, respectively. Eight CK23-35 resin cartridges were used for the anchorage of the roof cables.

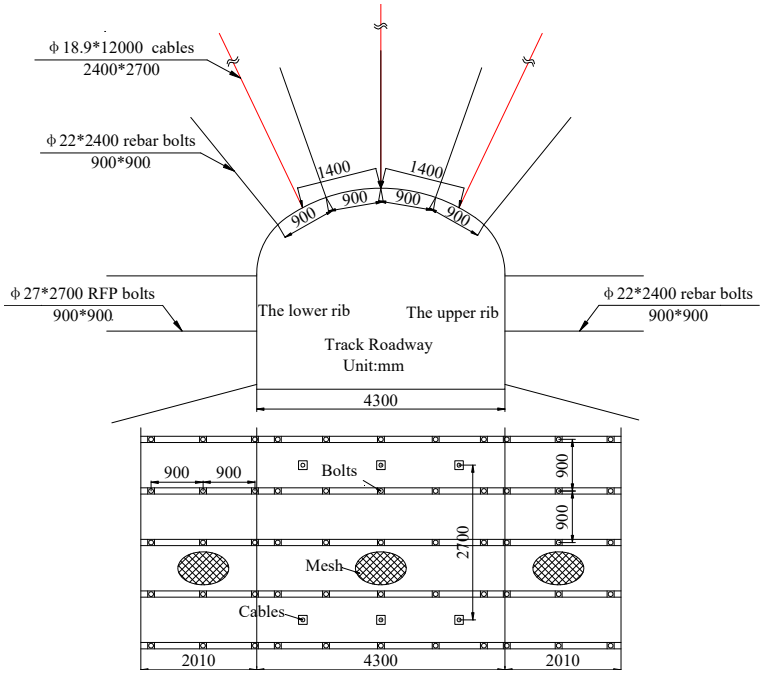

Fig. 20. The optimal bolting scheme of the track roadway under multi-seam mining

6. Field application results

6.1. Bolting costs

The number of bolting materials used in a section and their prices are shown in TABLE 6. The costs of the bolting materials in the primary bolting scheme and the optimal bolting scheme are shown in TABLE 7. Taking into account the type of bolt, cable, and anchoring agent, the cost of the optimal bolting scheme is 25.2% lower than that of the primary bolting scheme.

TABLE 6

The amount and the price of the bolting materials in a section

Scheme	The number of bolting materials					The price of the bolting materials / yuan			
	Rebar bolt	FRP bolt	Cable	Resin cartridge for bolts	Resin cartridge for cables	Rebar bolt	FRP bolt	Cable	Resin cartridge
The primary scheme	13	—	2	39	16	57.6	—	225.6	2.0
The optimal scheme	8	3	2	68	24	46.1	28.1	225.6	2.0

TABLE 7

The cost of the bolt schemes

Scheme	The cost of bolts in a single row / yuan	The rows of bolts	The cost of cables in a single row / yuan	The rows of cables	The total cost / yuan	The total cost per meter / yuan	Variation
The primary scheme	826.8	1506	483.2	502	1488000	1234.6	—
The optimal scheme	589.1	1340	724.8	447	1113000	923.7	–25.2%

6.2. Bolting effect

The plastic zones and the displacement of the track roadway under the optimal bolting scheme are shown in Fig. 21. In contrast to the primary bolting scheme in Fig. 16(a) and Fig. 17(a), the plastic zone depth and the displacement both decreased significantly when using the optimal bolting scheme. The plastic zone depth in the roof, the lower rib, and the upper rib declined by 9%, 8%, and 17%, respectively. The displacement in the roof, the lower rib, and the upper rib declined by 39%, 37% and 18%, respectively.

The optimal bolting scheme in Fig. 20 was used in the field in the remaining track roadway, and the deformation on the roadway surface 10 days after the tunnelling is shown in Fig. 22. The optimal bolting scheme can decrease the deformation in the roof and the ribs significantly, and improve the stability of the roadway under multi-seam mining, which verifies the reliability of the results in this study.

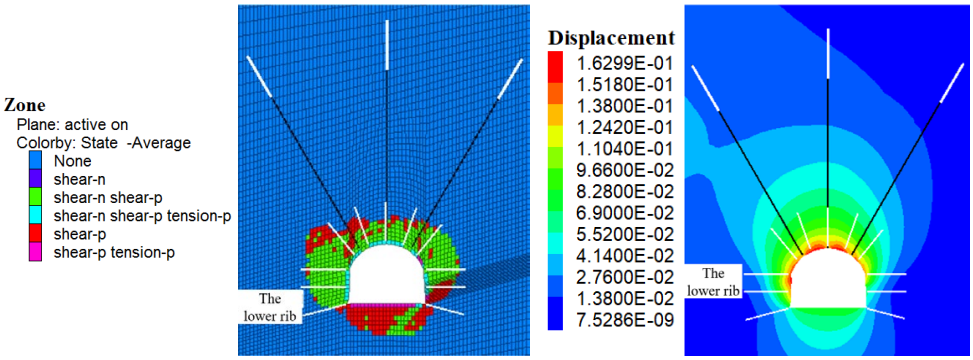

(a) Plastic zone (b) Displacement

Fig. 21. Plastic zone and deformation of the track roadway after the bolting scheme optimization

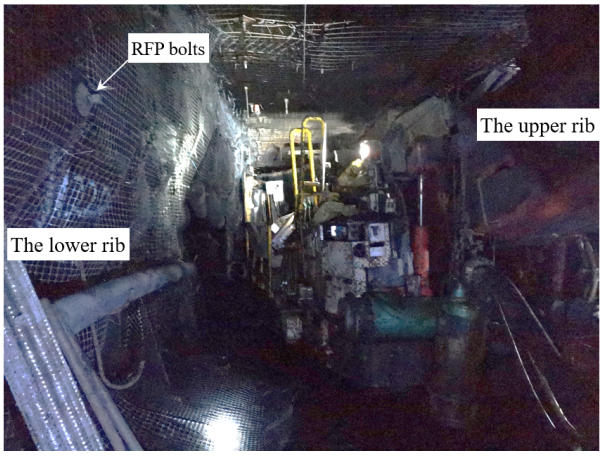

Fig. 22. Bolting effect in the track roadway under the optimal bolting scheme

7. Conclusions

As for the bolting control of the roadway under multi-seam mining, numerical simulation, laboratory test and field monitoring were conducted to study the stress field of the roadway under multi-seam mining, the anchorage performance of FRP and rebar bolts and the optimal bolting parameters. The main conclusions and findings are as follows.

(1) The spatial-temporal characteristics of the multi-seam mining in a mine were determined, and the stress field evolution of a track roadway under multi-seam mining was numerically analysed. The mining of the overburden of the 4-5# coal seam reduces the stress in the track roadway, thereby having a pressure-relief effect. During the mining of the overburden of the 9-10# and 14# coal seams, the stress in the track roadway increases significantly, and its concentration coefficient reaches 2.87. As a result of the overburden goafs and coal pillars, the track roadway is in a non-uniform stress field, in which the

stress in the roof and the lower rib is higher, while the stress in the floor and the upper rib is lower.

(2) The mechanical properties of FRP bolts and rebar bolts and their anchorage performance under different anchorage conditions were tested, and the stress distribution in the bolts with different anchoring types was monitored on-site. The tensile force of the 27 mm-diameter FRP bolt is 1.2 times that of the 22 mm-diameter rebar bolt. The shear strength of the full-length-anchored FRP bolt is 70.8 % higher than that of the end-anchored bolt, and the FRP bolt can serve the purpose of bolting the test roadway. Compared with the end-anchored bolts, the full-length anchorage system is confronted with axial tension as well as compression and shear force caused by mutual sliding between the broken coal and rock mass. The peak stress of the full-length anchored bolt is located in the shallow coal and rock mass. The full-length anchorage bolting system can effectively improve the stability of the roadway.

(3) The deformation and failure characteristics of a roadway with different bolting parameters under multi-seam mining were comparatively analysed, and finally, the optimised bolting scheme of the track roadway in the I011501 working face was determined. Five and three full-length anchored rebar bolts of Φ22 × 2400 mm were used in the roof and the upper rib, respectively, three full-length anchored FRP bolts of Φ27 × 2700 mm were used in the lower rib, and the spacing between the bolts was 900 × 900 mm. Three anchor cables of Φ18.9 × 12000 mm were used in the roof, and the spacing between the rows was 1400 × 2700 mm.

(4) The cost of the primary and optimal bolting schemes was calculated, and the bolting effect of the optimal bolting scheme was determined through numerical simulation and field application. The cost of the optimised bolting scheme is lower by about 25.2% as compared to the primary bolting scheme. The optimised bolting scheme can significantly reduce the deformation and plastic failure of the track roadway in the I011501 working face that is subject to multi-seam mining.

Multiple mining disturbances and new bolting materials were involved in the bolting control of the case roadway under multi-seam mining. The results can provide significant reference for the supporting control of roadway under similar conditions. It is worth noting that more field tests about the evolution of plastic zones around the roadway under mining-induced disturbance and the pull-out force of FRP and rebar bolts with different anchorage conditions are suggested to be conducted.

Acknowledgements

It should be noted that the work is financed by the National Natural Science Foundation of China (52304197), Key Laboratory of Safety and High-efficiency Coal Mining, Ministry of Education (JYBSYS202301), Scientific Research Foundation of High-level Talents of Anhui University of Science and Technology (2022yjrc38), Engineering Laboratory for Safe and Precise Coal Mining of Anhui Province (ESCMP202307).

References

[1] Z.H. Cheng, H. Pan, Q.L. Zou, Z.H. Li, L. Chen, J.L. Cao, K. Zhang, Y.G. Cui, Gas flow characteristics and optimization of gas drainage borehole layout in protective coal seam mining: A case study from the Shaqu coal mine, Shanxi Province, China. Natural Resources Research **30** (2), 1481-1493 (2021). DOI: https://doi.org/10.1007/s11053-020-09775-4

[2] C.K. Chabedi, T. Zvarivadza, Multi-seam mining of the deep Waterberg resources. Journal of The Southern African Institute of Mining and Metallurgy **116** (11), 1037-1042 (2016). DOI: https://doi.org/10.17159/2411-9717/2016/v116n11a5

[3] B. Ghabraie, G. Ren, J.V. Smith, Characterising the multi-seam subsidence due to varying mining configuration, insights from physical modelling. International Journal of Rock Mechanics and Mining Sciences **93**, 269-279 (2017). DOI: https://doi.org/10.1016/j.ijrmms.2017.02.001

[4] Q.D. Qu, H. Guo, K. Manoj, Monitoring and analysis of ground movement from multi-seam mining. International Journal of Rock Mechanics and Mining Sciences **148**, 104949 (2021). DOI: https://doi.org/10.1016/j.ijrmms.2021.104949

[5] A.A. Isachenko, M.G. Koryaga, Support and stabilization of temporary roadways in extraction of coal measures in Kuzbass. Journal of Mining Science **59** (3), 417-423 (2023). DOI: https://doi.org/10.1134/S1062739123030080

[6] J.G. Ning, J. Wang, Y.L. Tan, L.S. Zhang, T.T. Bu, In situ investigations into mining-induced overburden failures in close multiple-seam longwall mining: A case study. Geomechanics and Engineering **12** (4), 657-673 (2017). DOI: https://doi.org/10.12989/gae.2017.12.4.657

[7] B. Ghabraie, G. Ren, J.V. Smith, Characterising the multi-seam subsidence due to varying mining configuration, insights from physical modelling. International Journal of Rock Mechanics and Mining Sciences **93**, 269-279 (2017). DOI: https://doi.org/10.1016/j.ijrmms.2017.02.001

[8] B. Ghabraie, K. Ghabraie, G. Ren, J.V. Smith, Numerical modelling of multistage caving processes: insights from multi-seam longwall mining-induced subsidence. International Journal for Numerical and Analytical Methods in Geomechanics **41** (7), 959-975 (2017). DOI: https://doi.org/10.1002/nag.2659

[9] Q.X. Huang, J.W. Du, J. Chen, Y.P. He, Coupling control on pillar stress concentration and surface cracks in shallow multi-seam mining. International Journal of Mining Science and Technology **31** (1), 95-101 (2021). DOI: https://doi.org/10.1016/j.ijmst.2020.12.019

[10] C.L. Tian, X.L. Yang, H.T. Sun, Y.B. Liu, Q.T. Hu, Experimental study on the overburden movement and stress evolution in multi-seam mining with residual pillars. Energy Science & Engineering **7**, 3095-3110 (2019). DOI: https://doi.org/10.1002/ese3.482

[11] Z.Q. Liu, X.X. Zhong, B.T. Qin, H.W. Ren, A. Gao, Redevelopment of fractures and permeability changes after multi-seam mining of shallow closely spaced coal seams. Archives of Mining Sciences **64** (4), 671-686 (2019). DOI: https://doi.org/10.24425/ams.2019.129376

[12] D. Adhikary, M. Khanal, C. Jayasundara, R. Balusu, Deficiencies in 2D simulation: A comparative study of 2D versus 3D simulation of multi-seam longwall mining. Rock Mechanics and Rock Engineering **49** (6), 2181-2185 (2016). DOI: https://doi.org/10.1007/s00603-015-0842-7

[13] A.M. Suchowerska, J.P. Carter, R.S. Merifield, Horizontal stress under supercritical longwall panels. International Journal of Rock Mechanics and Mining Sciences **70**, 240-251 (2014). DOI: https://doi.org/10.1016/j.ijrmms.2014.03.009

[14] M.W. Zhang, S. Hideki, S. Takashi, M. Kikuo, L.M. Dou, Evolution and effect of the stress concentration and rock failure in the deep multi-seam coal mining. Environmental Earth Sciences **72**, 629-643 (2014). DOI: https://doi.org/10.1007/s12665-013-2985-8

[15] J. Wang, J.G. Ning, Y.L. Tan, S.C. Hu, W.Y. Guo, Deformation and failure laws of roadway surrounding rock and support optimizationduring shallow-buried multi-seam mining. Geomatics, Natural Hazards and Risk **11** (1), 191-211 (2020). DOI: https://doi.org/10.1080/19475705.2020.1713914

[16] N. Ghosh, H. Agrawal, S.K. Singh, G. Banerjee, Optimum chain pillar design at the deepest multi-seam longwall workings in India. Mining Metallurgy & Exploration **37** (2), 651-664 (2020). DOI: https://doi.org/10.1007/s42461-019-00138-z

[17] N.L. Pedersen, Overall bolt stress optimization. Journal of Strain Analysis for Engineering Design **48** (3), 155-165 (2013). DOI: https://doi.org/10.1177/0309324712470233

[18] V. Sarfarazi, K. Asgari, M. Nasrollahi, Interaction between rock bolt and rock bridge under tensile loading. Geomechanics and Engineering **25** (6), 455-471 (2013). DOI: https://doi.org/10.12989/gae.2021.25.6.455

[19] K. Yang, Y. Bai, C.T. Ding, S.Y. Kong, Comparative study on mechanical performance of bolted joints with steel and fibre reinforced polymer bolts. Journal of Building Engineering **41**, 102457 (2021). DOI: https://doi.org/10.1016/j.jobe.2021.102457

[20] T. Majcherczyk, Z. Niedbalski, P. Małkowski, L. Bednarek, Analysis of yielding steel arch support with rock bolts in mine roadways stability aspect. Archives of Mining Sciences **59** (3), 641-654 (2014). DOI: https://doi.org/10.2478/amsc-2014-0045

[21] R.A. Moffat, J.F. Beltran, R. Herrera, Applications of BOTDR fiber optics to the monitoring of underground structures. Geomechanics and Engineering **9** (3), 397-414 (2015). DOI: https://doi.org/10.12989/gae.2015.9.3.397

[22] J.P. Zhang, L.M. Liu, C.X. Liu, Y. Li, Mechanism and application of new prestressed yield bolt for controlling deep high-stress rock mass. Tunnelling and Underground Space Technology **119**, 104254 (2022). DOI: https://doi.org/10.1016/j.tust.2021.104254

[23] P. Małkowski, X.W. Feng, Z. Niedbalski, M. Żelichowski, Laboratorial tests and numerical modeling of rock bolts bonded by different materials. Rock Mechanics and Rock Engineering **56** (4), 2589-2606 (2023). DOI: https://doi.org/10.1007/s00603-022-03191-1

[24] B.J. Sun, Q.W. Liu, W.T. Li, X.Z. Yang, B. Yang, T.C. Li, Numerical implementation of rock bolts with yield and fracture behaviour under tensile-shear load. Engineering Failure Analysis **139**, 106462 (2022). DOI: https://doi.org/10.1016/j.engfailanal.2022.106462

[25] N. Lawler, M.A. Polak, Development of FRP shear bolts for punching shear retrofit of reinforced concrete slabs. Journal of Composites for Construction **15** (4), 591-601 (2011). DOI: https://doi.org/10.1061/(asce)cc.1943-5614.0000188

[26] D.S.E. Abdelkerim, X. Wang, H.A. Ibrahim, Z.S. Wu, Static and fatigue behavior of pultruded FRP multi-bolted joints with basalt FRP and hybrid steel-FRP bolts. Composite Structures **220**, 324-337 (2019). DOI: https://doi.org/10.1016/j.compstruct.2019.03.085

[27] J. Han, Z.Q. Bi, B. Liang, C. Cao, S.W. Ma, Anchorage performance of large-diameter FRP bolts and their application in large deformation roadway. International Journal of Mining Science and Technology **33**, 1037-1043 (2023). DOI: https://doi.org/10.1016/j.ijmst.2022.09.028

[28] J. Feng, R.X. Wang, Y.F. Zhang, Z.N. Tu, T. Yang, Examining the creep characteristics of basalt fiber-reinforced polymer grouted bolts in mixed soil. International Journal of Geomechanics **23** (10), 04023164 (2023). DOI: https://doi.org/10.1061/ijgnai.gmeng-8355

[29] T. Nguyen, K. Ghabraie, T.C. Thanh, Simultaneous pattern and size optimisation of rock bolts for underground excavations. Computers and Geotechnics **66**, 264-277 (2015). DOI: https://doi.org/10.1016/j.compgeo.2015.02.007

[30] S. Ghyasvand, A. Fahimifar, F.M. Nejad, On the optimum design of reinforcement systems for old masonry railway tunnels. Geomechanics and Engineering **28** (2), 145-155 (2022). DOI: https://doi.org/10.12989/gae.2022.28.2.145

[31] Itasca Consulting Group. Inc. Fast Language Analysis of Continua in Three Dimensions Versin 6.0 User's Manual. USA: Itasca Consulting Group, Inc.; 2017.